Experimental benchmark and code validation for airfoils equipped with passive vortex generators

Baldacchino, Daniel; M Manolesos, M.; Simao Ferreira, Carlos; Gonzalez Salcedo, A; Aparicio, M.; Chaviaropoulos, T.; Diakakis, K.; Florentie, Liesbeth; Garcia, M.; Papadakis, G

DOI
10.1088/1742-6596/753/2/022002

Publication date
2016

Document Version
Final published version

Published in
Pramana: journal of physics

Experimental benchmark and code validation for airfoils equipped with passive vortex generators

2016 J. Phys.: Conf. Ser. 753 022002

(http://iopscience.iop.org/1742-6596/753/2/022002)

Experimental benchmark and code validation for airfoils equipped with passive vortex generators

D Baldacchino[1], M Manolesos[2], C Ferreira[1], Á González Salcedo[3], M Aparicio[3], T Chaviaropoulos[2], K Diakakis[2], L Florentie[1], N R. García[4], G Papadakis[2], N N. Sørensen[4], N Timmer[1], N Troldborg[4], S Voutsinas[2] and A van Zuijlen[1]

[1]DUWIND, Faculty of Aerospace Engineering, Delft University of Technology, Kluyverweg 1, 2629HS Delft, The Netherlands
[2]Laboratory of Aerodynamics, National Technical University of Athens, Greece
[3]CENER - National Renewable Energy Centre, Ciudad de la Innovación 7, Sarriguren, Navarra, 31621, Spain
[4]Technical University of Denmark, Department of Wind Energy, RisøCampus, Frederiksborgvej 399, 4000 Roskilde Denmark

E-mail: [1]d.baldacchino@tudelft.nl (D Baldacchino), [2]marinos@fluid.mech.ntua.gr (M Manolesos)

Abstract. Experimental results and complimentary computations for airfoils with vortex generators are compared in this paper, as part of an effort within the AVATAR project to develop tools for wind turbine blade control devices. Measurements from two airfoils equipped with passive vortex generators, a 30% thick DU97W300 and an 18% thick NTUA T18 have been used for benchmarking several simulation tools. These tools span low-to-high complexity, ranging from engineering-level integral boundary layer tools to fully-resolved computational fluid dynamics codes. Results indicate that with appropriate calibration, engineering-type tools can capture the effects of vortex generators and outperform more complex tools. Fully resolved CFD comes at a much higher computational cost and does not necessarily capture the increased lift due to the VGs. However, in lieu of the limited experimental data available for calibration, high fidelity tools are still required for assessing the effect of vortex generators on airfoil performance.

1. Introduction and research motivation

The wind energy sector continues to grow with every passing year, as do the state-of-the-art rotors that populate new wind farms. In fact, wind turbines are approaching the 10MW mark and the current longest blades span 80m [1]. The sheer size of these machines is pushing engineering design tools to the edge of their intended envelope of validity. Thus, AdVanced Aerodynamic Tools for lArge Rotors (AVATAR) [2] require renewed attention.

A classical problem encountered on rotating wind turbine blades is flow separation, which leads to lower airfoil efficiency, reduced power output, as well as increased fatigue damage by virtue of its unsteady nature. Dynamic stall and inflow, blade interaction with incoming turbulence and soiling can all lead to premature separation. The larger the rotor, the more pronounced these issues generally become as the rotor samples a larger wind field. Additionally, blade root connections need to withstand significant loads, placing more stringent structural

requirements on the blades, such as thicker root sections. Flow separation occurs more readily on thick airfoils due to the stronger adverse pressure gradients. However, the ability of a flow to negotiate these non-ideal conditions can be improved passively with vane-type vortex generators (VGs).

The interaction of a vortex with a boundary layer can enhance streamwise momentum close to the wall and thus prevent or delay flow separation. Thick airfoil sections then, could particularly benefit from such devices. VGs may also be used to circumvent roughness-induced separation, a known issue with field turbines [3]. However, these blade "add-ons" present new design and modelling challenges, such as (*i*) correctly capturing the effect of vortex-enhanced mixing on airfoil characteristics, and (*ii*) doing so in cost-effective manner, suitable for design iteration. There is a large number of parameters of interest in the study of vortex generators. These are mainly the chord-wise position of the VGs, the size of the VG, aspect ratio (AR), inclination and the inter- and intra-spacing of the VG pairs (shown in Figure 1). Since the typical height of a VG is similar to the local boundary layer thickness δ, even finer details must be resolved close to the wall compared to uncontrolled configurations.

There are ample experimental studies on VGs [4], initiated in large part by the aeronautical sector for improving aircraft wing performance (external flows), as well as for internal flows such as turbine ducts, diffusers and intakes [5]. The modelling of VGs has also been an important and recurring research topic. Apart from a few isolated studies employing expensive DNS/LES type calculations [6, 7], RANS-based approaches are by far the most common. A popular method of simplifying VG modelling was pioneered by Bender [8] and extended by Jirasek [9]. Here, the VG was indirectly modelled by introducing a local flow-dependent forcing term to the momentum and energy equations. The side forces generated in this manner are approximated from thin airfoil theory and are mildly dependent on a (geometry-related) calibration coefficient [8]. This effectively triggers the rollup and development of a streamwise vortex whilst alleviating the dense grid requirements of fully resolved (FR) geometries. Statistical and analytical models have also been developed [10, 11]. Intermediate methods based on the robust integral boundary layer (IBL) method were explored by NASA in 2003, modifying the widely used XFOIL code to incorporate the effect of VGs [12]. Engineering approaches are also possible [13]; however, these rely heavily on empirical data and are probably not robust enough for design purposes.

From an engineering standpoint, parametric exploration is an important aspect for design. Tools therefore must be assessed for their robustness and ability to capture the trends of equipping airfoils with VGs. For this purpose, the current paper will benchmark different RANS and an in-house IBL code against airfoil measurements with and without vortex generators [14, 15]. The experimental data used for this validation study concerns the Delft-designed 30% thick DU97W300 airfoil and an 18% NTUA T18 airfoil.

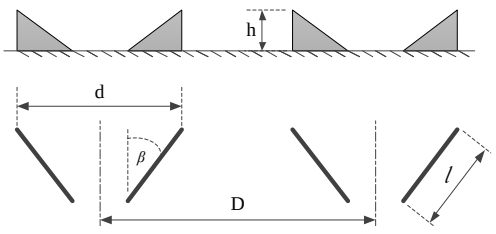

Figure 1: Frontal (top, shaded) and planar (bottom) schematic of the periodic VG-array arrangement and nomenclature

2. Experimental database and numerical tools

2.1. Experimental airfoil data

The DU97W300 airfoil model was tested in the Low Turbulence Tunnel at the Delft University of Technology and detailed in Timmer et al. [16]. The model chord length is 0.65m and features a "thick" trailing edge (TE) of approximately 1.7% chord. The data used for validation was obtained at a chord Reynolds number, $\mathrm{Re}_c = 2 \cdot 10^6$ (Mach No. = 0.13). Polars were acquired in the freely transitional regime, as well as for forced transition using zig-zag (ZZ) tape (11mm wide, 0.35mm thick) at 5% chord.

The NTUA T18 model was analysed in the wind tunnel at the National Technical University of Athens and reported by Manolesos et al. [17] at $Re_c = 0.87 \cdot 10^6$ (Mach No. = 0.07). The airfoil model has a chord length of 0.60m. Polars and pressure distributions were acquired for a fully turbulent (tripped) flow. This was enforced using ZZ tape (12mm wide, 0.40mm thick) at 2% chord over the central section of model [18].

For both experiments, the height of the roughness used is considered oversized for minimum tripping requirements at the tested Re numbers [3, 16, 19]. The DU and NTUA airfoils were fitted with counter-rotating, passive vane-type VGs sized to the boundary layer height in common-downwash and upwash configuration respectively. The VGs were optimised to produce the highest C_L/C_D. Moving the VGs further aft can achieve this, but also limits the operational range and reduces $\alpha_{CL,max}$. A compromise is then necessary and is found in the current designs. For both cases, the VGs were manufactured from 0.2mm aluminium sheeting and arranged in array configuration, spanning the entire length of the models. Details of the experimental wing setups and VG configurations are summarised in Figure 2 and Table 1.

2.1.1. Experimental uncertainty In both setups, the lift and drag coefficients were obtained from integration of the airfoil static pressures, whereas profile drag is determined using wake-rake measurements, located downstream of the models. In such a setup, systematic errors may

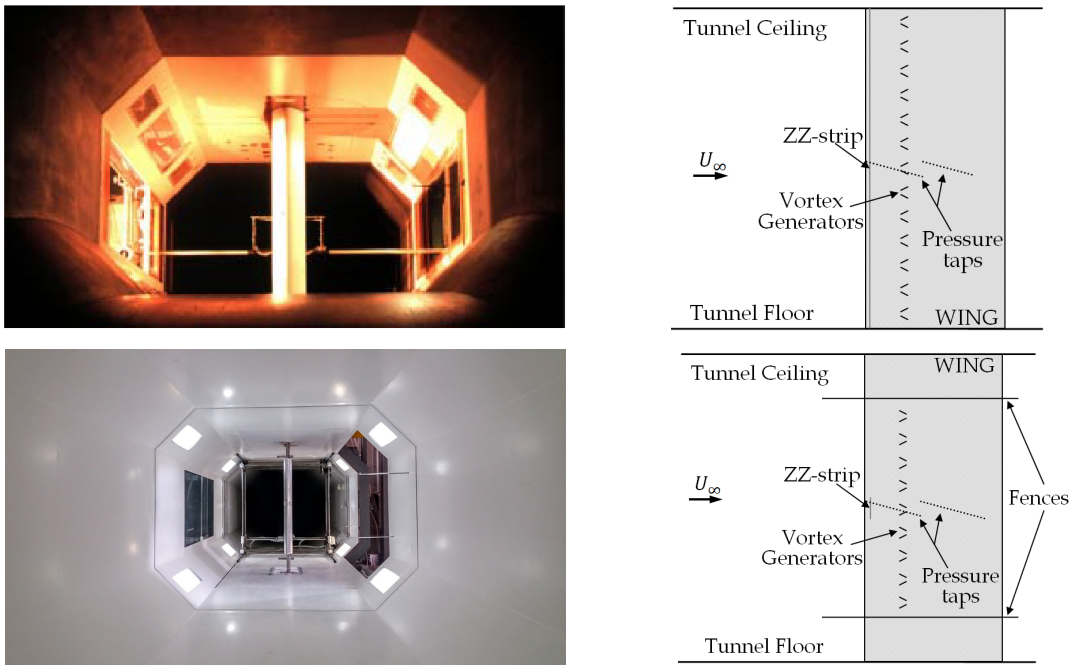

Figure 2: Test-section and setup schematic for the (*top*) DU97W300 airfoil [16] and (*top*) NTUA T18 airfoil (adapted from [17]).

Table 1: Flow facilities, airfoil models and VG parameter details used for benchmark

Airfoil	Wind Tunnel	Test Section L×B×H	Freestream turbulence intensity	Model pressures	Wing aspect ratio	Model solid blockage
DU97W300	Closed loop	$2.60m \times 1.80m \times 1.25m$	$< 0.1\%$ at $50m/s$	102 taps (staggered)	1.92	$\approx 10\%$ at $16°$
NTUA T18	Closed loop	$3.75m \times 1.80m \times 1.40m$	0.2%	60 taps	2.0	$\approx 9\%$ at $16°$

Airfoil	Thickness t/c [%]	Exp. Data Type[a]	Chordwise position, x/c [%]	Shape	Config.	h/δ	Vane Angle, β	Vane chord, l/h	Intra-vane spacing, d/h	Inter-vane spacing, D/h
DU97W300	30%	P/C_p	20%,30%	Delta	Ctr.[b]/CD[c]	1	16.4°	3.5	3.9	7.0
NTUA T18	18%	P/C_p	30%,40%	Delta	Ctr./CU[d]	1	20°	3	3.7	11.7

[a]P: Polar data, C_p: Pressure data; [b]Ctr.: Counter-rotating; [c]CD: Common-downflow; [d]CU: Common-upflow

arise from misalignments (e.g. zero angle offset), bias in pressure measurements, signal drift due to temperature effects and model manufacturing defects. Interference from adjacent pressure taps is minimised by staggering their spanwise distribution and keeping the orifice diameter small (< 1.0mm). These are minimised through careful design and reliable manufacturing methods.

Random errors are minimised by using high precision equipment. The DU-airfoil pressure measurements were acquired by an optical sensor coupled with a multi-tube liquid manometer. Diurnal variations of atmospheric temperature and pressure have a small influence on the density of the manometer fluid and resulting pressure level. Additionally, aerodynamic heating can raise the liquid temperature through contact with the bleed air. This can lead to signal drift if unaccounted for, although after some initial start-up period, these factors diminish. Uncertainty in the angle of attack is below 0.01 deg and the smallest resolution of the manometer is 0.1mm ($\approx$ 1Pa). The error propagation based solely on these factors results in an average uncertainty of ± 0.001 for C_p, ± 0.005 on C_L and ± 0.0003 on C_D. This corresponds to a worst-case 1% error on lift and drag. Flow separation on the surface results in fluctuating wall and wake pressures. In this case multiple readings are taken and averaged. However, the liquid manometer and connective tubing inherently damp out pressure fluctuations, and so to some extent naturally indicate averaged readings and reduce sampling errors. NTUA pressure measurements were acquired through a Furness scanner and read through a manometer and Scanivalve pressure transducer. This set of measurements carries an uncertainty of 0.02 deg on the angle of attack, ± 0.0002 on C_p, ± 0.0007 on C_L and ± 0.0004 on C_D.

Wind tunnel corrections are an additional source of uncertainty. These are applied to both models and take into account wall and model blockage, as well as streamline curvature. However, in the immediate post stall-regions, wind tunnel airfoil flows are typically characterised by corner separation and stall cell formation, leading to a highly three-dimensional flow structure along the span [19]. Thus the model surface pressures in the post-stall region should be interpreted with caution as they are likely not indicative of the spanwise averaged flow. The periodic placement of VGs gives rise to spanwise-periodic flow and loading. For the wake-rake drag, the periodicity is addressed by spanwise averaging values taken at different spanwise positions along a VG array wavelength. An equivalent approach is by definition applied to the 3D computations for both drag and lift (see next section). However, experimentally, the true spanwise-averaged lift is not-possible due to the staggering of the pressure taps. Only by repeating measurements with different relative VG array positions to the pressure taps, or balance measurements, can a more indicative value of for the spanwise average lift be obtained.

2.2. Numerical tools

All CFD codes are based on finite-volume solvers and have been run for an incompressible, steady flow. The uncontrolled cases have been computed in 2D whilst all VG cases were computed on a half-pair strip (hereafter referred to as 'low AR 3D'), imposing spanwise-periodic boundary conditions on the domain side walls. All codes use different, uniquely generated grids which ensure $y^+ < 2$, fully resolving the boundary layer. Except for fully-resolved CFD VG simulations, the vanes are considered zero-thickness. Grid independence is ensured and only the finest grid results are presented here. An overview of the predictive tools is given in Table 2 and detailed below.

DTU computations were performed using the in-house EllipSys RANS solver [21, 22, 23]. Convective terms are discretized using the QUICK scheme, as given by [24]. The turbulent simulations are carried out using Menter's k-ω SST model described in [25], while the transitional simulations are based on the e^N transition model as described in [26]. Along with simplified BAY-type simulations, fully-resolved VG computations were also performed on a single VG vane with imposed spanwise periodic boundary conditions to mimic the array effect.

Q^{3}UIC is a Quasi-three dimensional Unsteady Interactive boundary layer Code built on a viscous-inviscid interaction technique, developed by Ramos-García et al. at DTU [20]. This code uses a strong coupling between the viscous and inviscid parts via the transpiration velocity concept. The outer inviscid part is modelled by a two-dimensional panel method, and the viscous part is modelled by solving the integral form of the laminar and turbulent boundary layer equations. Transition can be forced by employing a boundary-layer trip or computed freely using the e^N envelope transition method with Mack's modification to account for the turbulent intensity [27]. VGs are modelled based on the approach of Kerho [12]. A source term is added to the the shear-stress transport equation, effectively increasing the production of turbulence and mass entrainment from the VG location in a decreasing fashion, mimicking the formation and eventual decay of an embedded vortex.

NTUA calculations were performed using the in-house MaPFlow code, a multi-block compressible solver equipped with preconditioning in regions of low Mach flow [28]. The discretization scheme is cell centered and makes use of the Roe approximate Riemann solver for the convective fluxes. In space, the scheme is 2nd order accurate, defined for unstructured grids. Turbulence is also modelled using the k-ω SST model. The effect of VGs is simulated by means of the BAY model [8], with jBAY [9] refinements, in which the VG is replaced by a surface with zero thickness.

The second NTUA approach for VG modelling is based on a phenomenological model proposed by Nikolaou et al. [29] and builds on the MaPFlow code. An explicit VG model is used which is based on the superposition of a vortex flow field on the Navier-Stokes equations. A spanwise averaging operation then simplifies the system to a two-dimensional viscous flow problem with additional source terms and fluxes representing the vortex flow field. A system of co- or counter-rotating vortex lines are released from the specified VG positions, and left to operate on the flow. These vortex filaments are assumed to follow the flow, which is mainly true except in the proximity of the VG.

TUDelft calculations were performed in OpenFOAM, an open source CFD software

Table 2: Partner contributions

Code	Developer	Type	Space	Turbulence	Transition	VG modelling	Grid Size
EllipSys	DTU	CFD	3D	k-ω SST	e^N	BAY/Fully-Resolved	$1-7\cdot10^6$
Q^{3}UIC	DTU	IBL	2D	Closure Relations [20]	e^N	Shear-lag correction	140 panels
MaPFlow	NTUA	CFD	3D	k-ω SST	–	BAY	$1\cdot10^6$
VGFlow	NTUA	CFD	2D	k-ω SST	–	Vortex model + RANS	$0.05\cdot10^6$
OpenFoam	TUDelft	CFD	3D	k-ω SST	–	BAY	$2-4\cdot10^6$

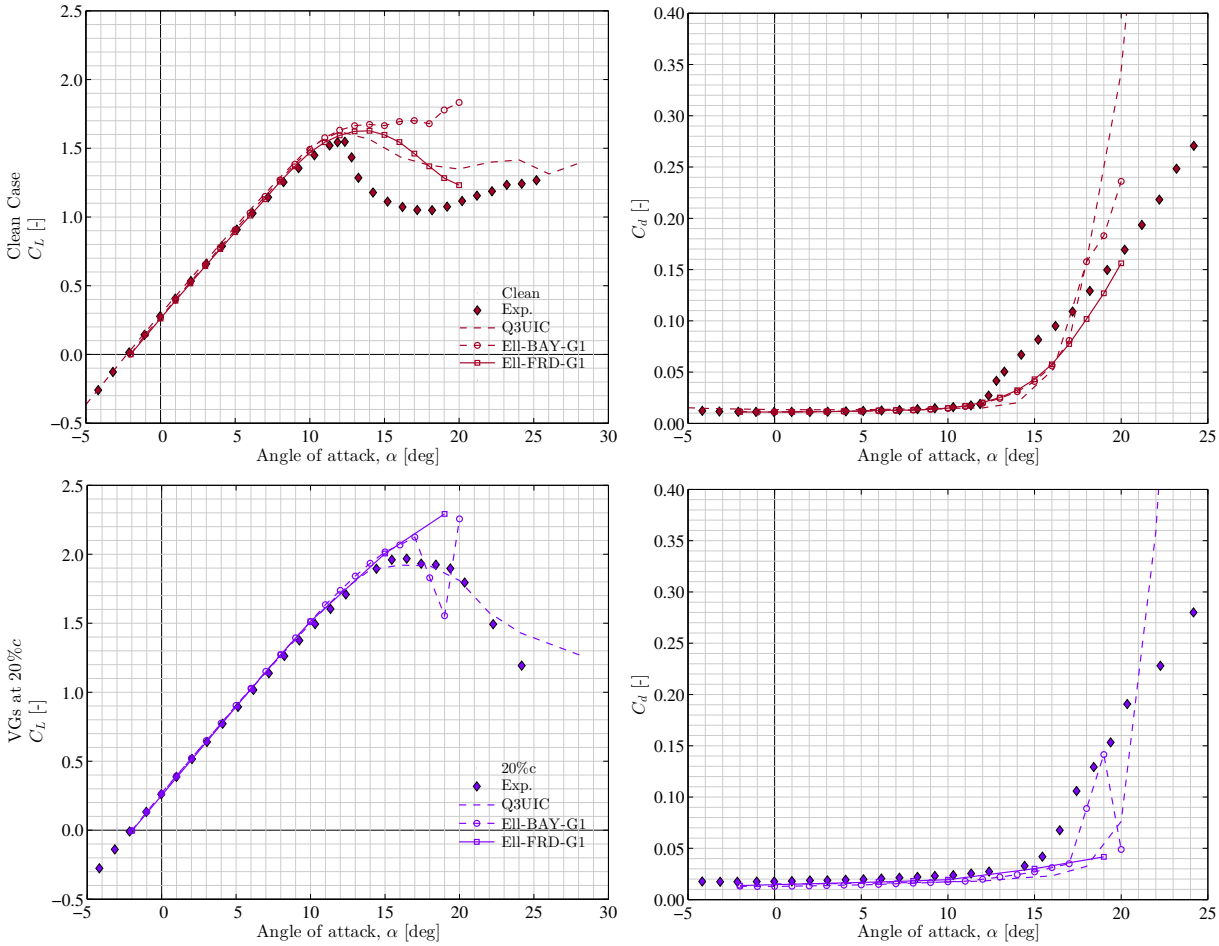

Figure 3: Lift and drag polars for transitional computations of the clean DU97W300 airfoil.

distributed under the General Public Licence (GPL), and detailed in Jasak [30]. OpenFoam is a segregated finite volume code able to solve compressible and incompressible flows. For this analysis, the steady, incompressible RANS equations are solved using the SIMPLE algorithm and the governing equations are solved using first order upwind discretization schemes for the convective terms. The fully turbulent simulations use Menter's two-equation k-ω SST model [25] for closure. VG simulations are conducted using a newly implemented BAY model in OpenFoam, detailed in Florentie et al. [31].

3. Benchmark results

3.1. DU97W300, 30%t/c, $Re = 2 \cdot 10^6$

First, the case without roughness is considered in Figure 3. The EllipSys and Q^{3}UIC codes are equipped with transitional models, and appear to capture the lift and drag characteristics very well without VGs. The drag prediction is very good, differences with experiments being close to the uncertainty level on the measurements. The maximum lift is within 6% of the measured value whereas the maximum lift angle is overpredicted by approximately 1° by EllipSys. Q^{3}IUC captures this peak more accurately. Both predictions overestimate the lift in the post-stall region and under-estimate the drag. Typically, prior to stall, a separated flow region starts forming from the trailing edge, and gradually grows forward as maximum lift is reached. This process is notoriously difficult for RANS and IBL codes to predict, especially considering that separation

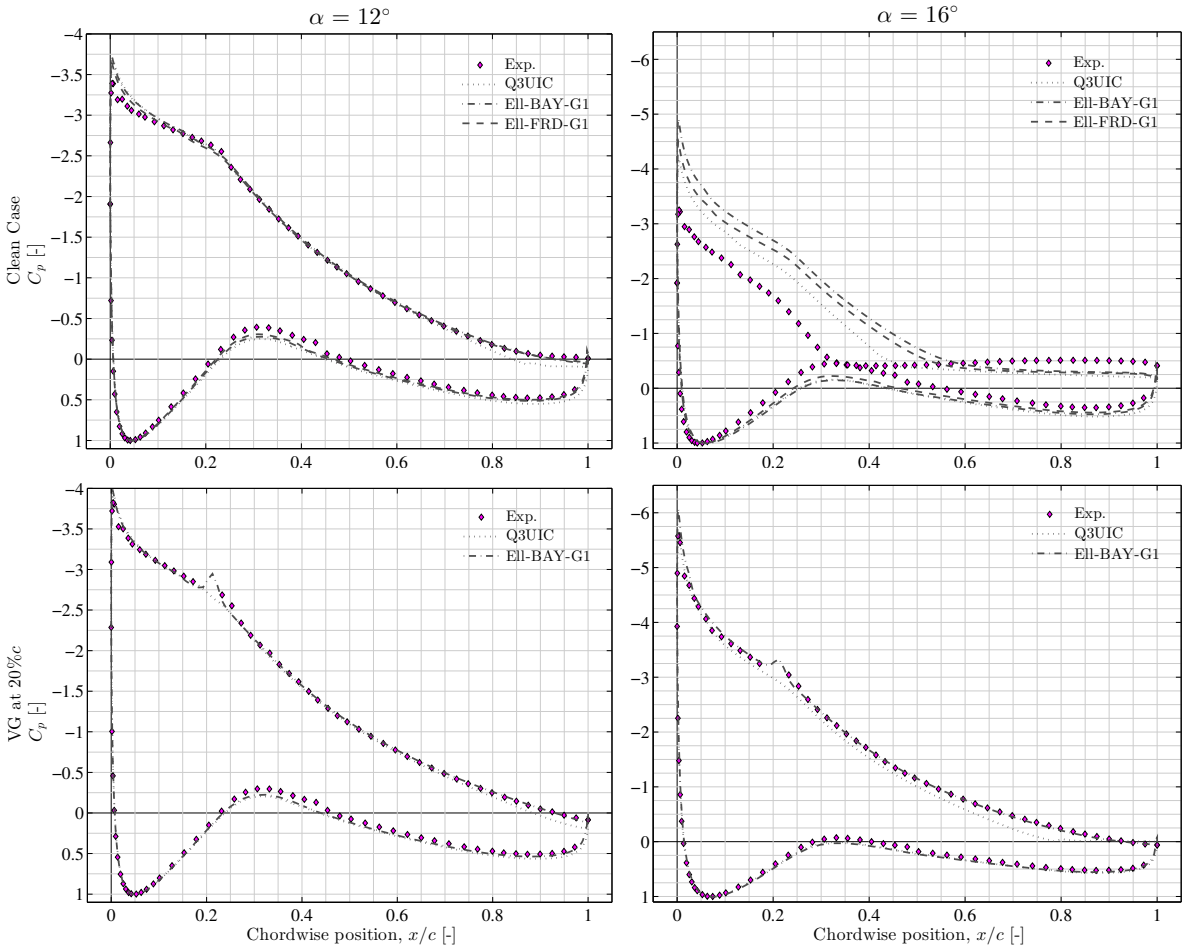

Figure 4: Pressure distributions for the DU97W300 airfoil in free transition; $C_p(x)$ for (*Left column*) $\alpha = 12°$ and (*right column*) $\alpha = 16°$ (Note different graph scale).

is in fact a 3D phenomenon. The pressure distributions highlight the performance in a region near $C_{L,max}$ and in the post-stall regime ($\alpha = 12°$ and 16°) in Figure 4. The slightly higher lift is explained by a higher suction peak and lower surface pressure around 30%c. In the post-stall regime, we see that the extent of separated flow (indicated by the pressure plateau on the suction side) is underestimated by the codes, thus predicting higher lift and lower drag, the latter now composed mainly of pressure drag.

With the addition of VGs at 20%c, $C_{L,max}$ is extended from 1.55 to 1.97, until $\alpha_{CL,max} = 16.5°$. With sufficient tuning, Q^{3}UIC captures this very well, albeit for a slightly lower $C_{L,max}$. EllipSys appears to overpredict the effect of the VGs, and both BAY and FR simulations perform similarly. The experimental drag in the linear region is slightly higher than computations, likely because of the parasitic drag from the VG base plate on the model. Apart from increasing the boundary layer thickness slightly, this is also has the effect of forcing transition at the leading edge (LE) of the plate, something which is not modelled in the computations. This also accounts for the slightly overestimated lift slope. The pressure distributions support these observations. Interesting to note is that Q^{3}UIC predicts the onset of TE separation over the aft 20%c at $\alpha = 16°$. This effectively de-cambers the airfoil, resulting in the lower suction peak and an overall shift in the pressure distribution on the upper side, resulting in lower lift. Note that after application of wind tunnel corrections, the effective measured angle of attack may differ

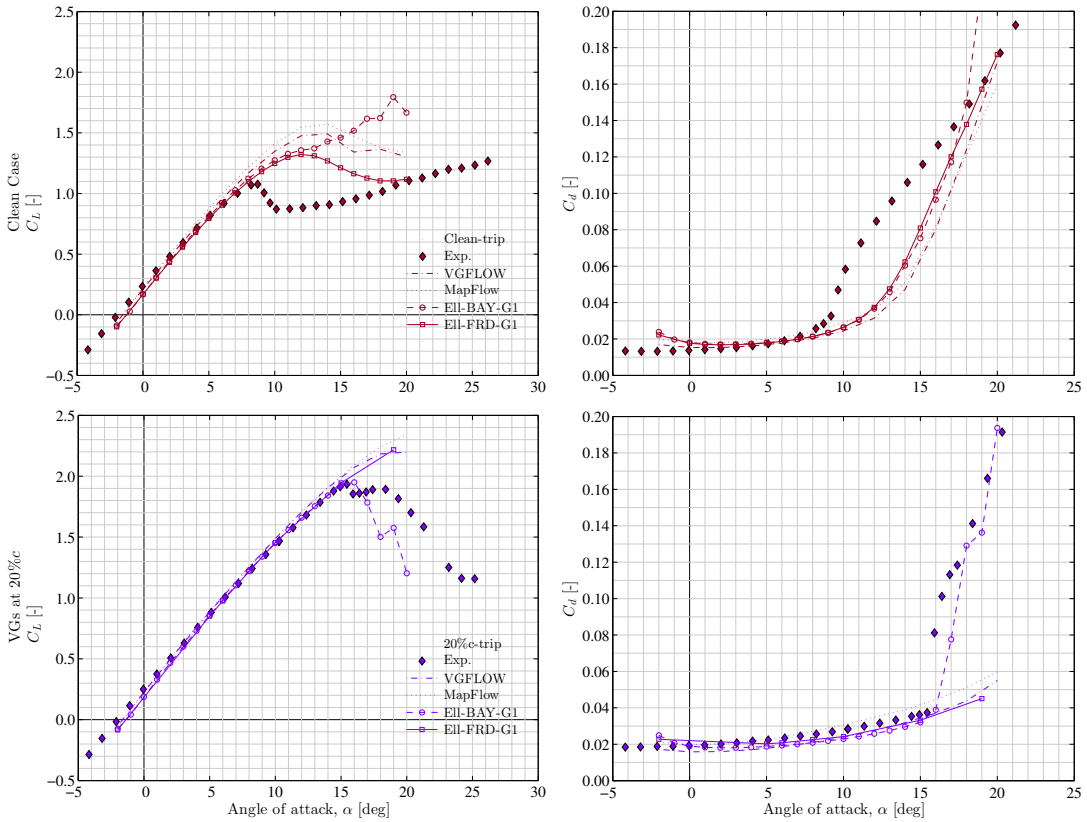

Figure 5: Lift and drag polars for turbulent computations of the tripped DU97W300 airfoil.

by up to $\pm 0.3°$ from the rounded geometric angle. However, computations were conducted at round integer values. Therefore, differences in the measured and predicted pressures are partly attributed to this small discrepancy.

A roughness case is also considered in Figure 5. For this case, computations are run with fully turbulent conditions. All codes over-predict the performance of the DU97W300 (without VGs). Van Rooij and Timmer [3] remarked that ZZ tape has a lower critical Reynolds number compared to other trip devices, making it an efficient tripping device. However, its presence still increases the boundary layer thickness [16] and appears to cause early turbulent separation, which the computations do not capture. The pressure distributions illustrate this further in Figure 6.

The presence of VGs counteracts the earlier turbulent separation by re-energising the flow downstream. For these reasons, the comparisons are more favourable with VGs since the issue of early turbulent separation is circumvented. With VGs at 20%c, $C_{L,max}$ and its corresponding angle of attack are captured rather well by the BAY-type EllipSys computations, albeit with sharper stalling behaviour compared with measurements. The remaining predictions overshoot $C_{L,max}$ and its location. VGFlow and MaPFlow perform similarly, and do not predict separation until higher angles of attack. The same can be said of FR EllipSys calculations. A BAY model has been implemented in MaPFlow and EllipSys, yet both predictions differ. The pressure distributions in Figure 6 show that MaPFlow predicts a higher suction peak and upper side pressure, even without VGs. The stepped post-stall characteristic in the measured lift polar is typical of 3D separation effects and is probably related to an intermittent interaction of separated flow regions with the streamwise vortices. However, the latter cannot be verified from the presented data without supporting flow field investigations. Drag predictions improve

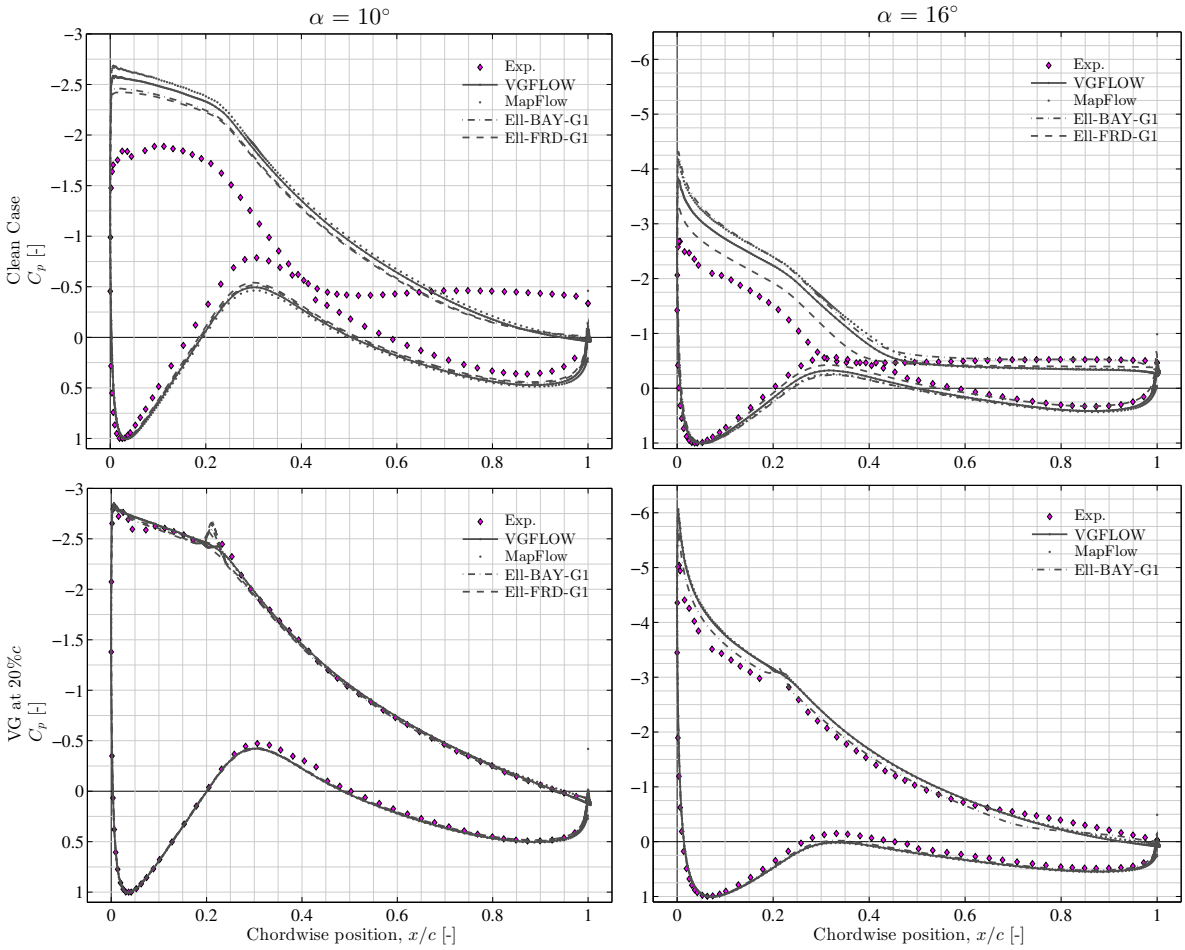

Figure 6: Pressure distributions for the turbulent (tripped) DU97W300 airfoil; $C_p(x)$ for (*Left column*) $\alpha = 10°$ and (*right column*) $\alpha = 16°$ (Note different graph scale).

slightly in the VG case with respect to the clean case due to the significant reduction in pressure drag from the ZZ strip. Pre-stall drag is predicted fairly well by all codes.

3.2. NTUA T18, 18%t/c, $Re = 0.87 \cdot 10^6$

A comparison of the lift and drag polars for the NTUA T18 airfoil is shown in Figure 7 for controlled and uncontrolled cases (all with roughness trips). The predictions capture the soft stalling characteristics in the clean case rather well, but at higher $C_{L,max}$. Results from all CFD codes are quite comparable until stall. The pressure distribution for the uncontrolled case for $\alpha = 12°$ and $16°$ in Figure 8 shows that the issue is related to the prediction of the separated region. MaPFlow again appears to overestimate the suction pressure distribution whereas Q^{3}UIC underestimates it over the aft 40%c.

In general, the results show higher spread with VGs, around $C_{L,max}$, but also with respect to the lift slope, again indicating possible effects of roughness trip height. Both BAY-type and FR simulations show an increased performance with VGs, as do the lower-complexity VGFlow and Q^{3}UIC, but over predict the VG effect compared to the experimental results. The EllipSys-BAY results appear to signal the abrupt stalling behaviour, albeit some degrees earlier than the steep drop in the measured lift. For $\alpha = 12°$, the experimental pressures do not indicate separation with VGs (no visible plateau), whereas Q^{3}UIC and EllipSys-BAY predict TE separation over the

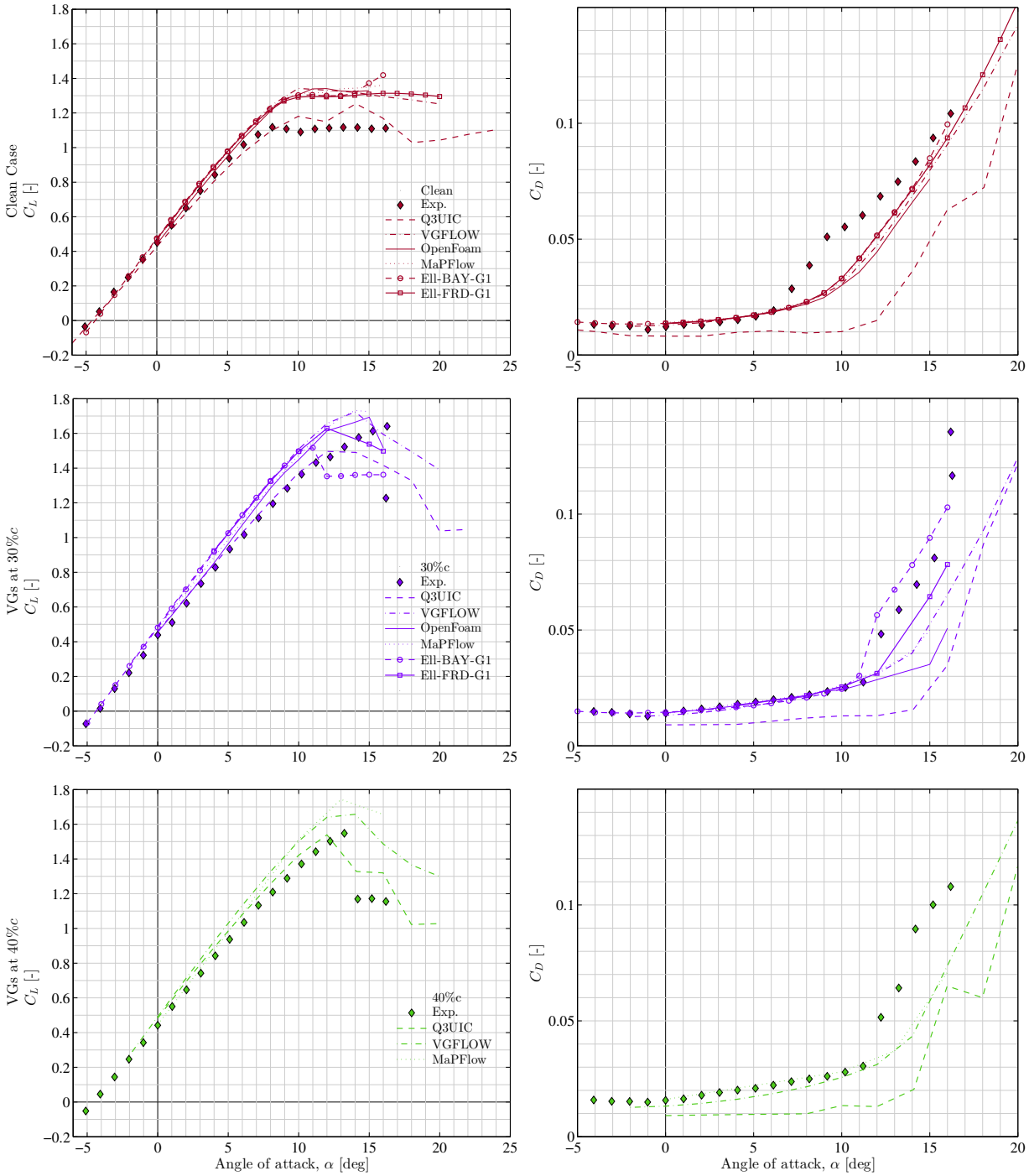

Figure 7: Lift and drag polars for computations of the NTUA T18 airfoil. Rows represent the Clean Case and VGs at 30%c and 40%c respectively (fully turbulent experiment and simulations).

aft $20-30\%$ chord. The computational meshes used in the EllipSys and OpenFoam simulations were generated on a noisy surface measurement of the actual wing model, which explains the fluctuating pressure values close to the LE (Figure 8). This is possibly the reason for the earlier stall in the EllipSys results.

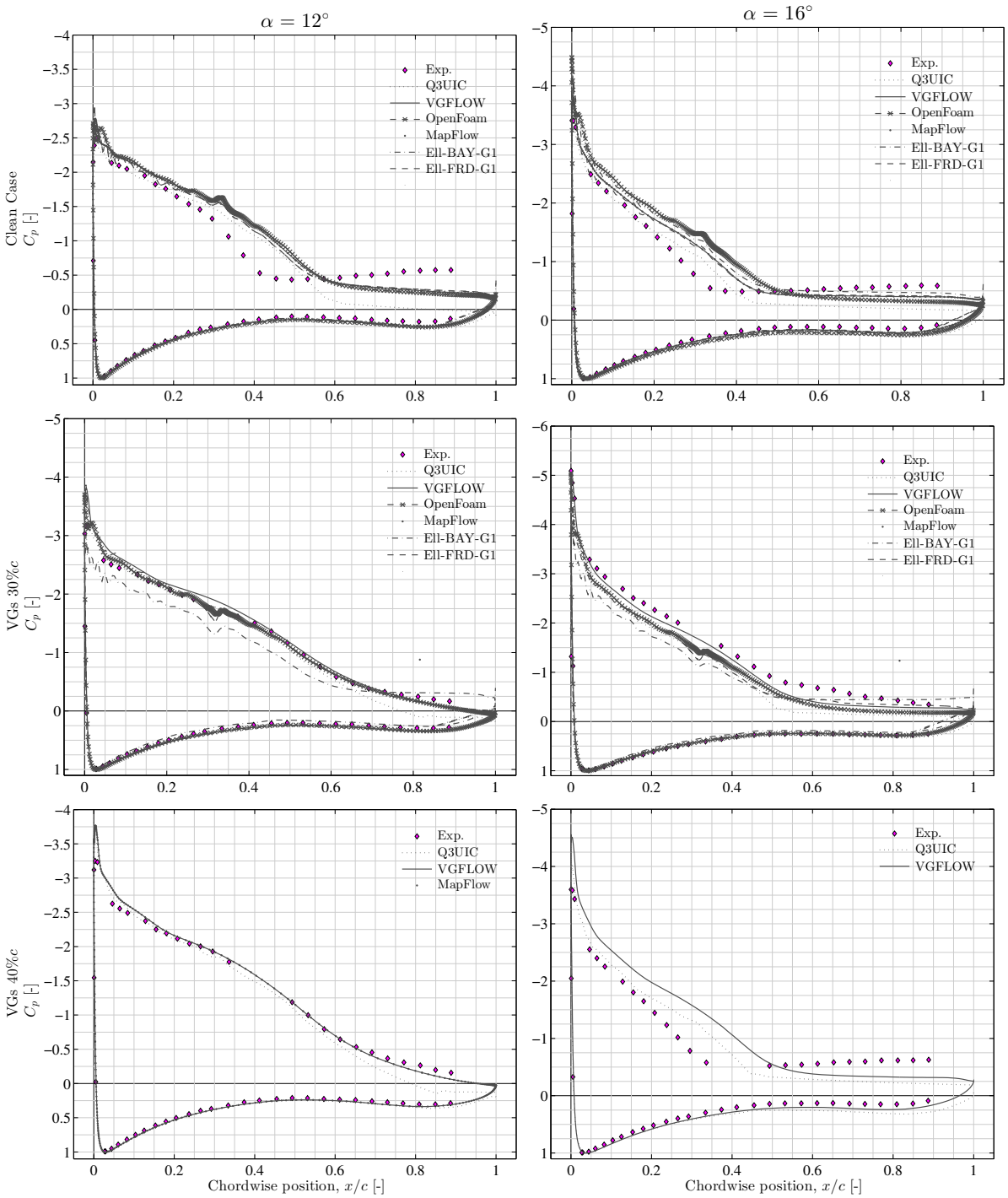

Figure 8: Pressure distributions for the NTUA T18 airfoil; $C_p(x)$ for (*Left column*) $\alpha = 12°$ and (*right column*) $\alpha = 16°$. Rows represent the Clean Case, VGs at 30%c and 40%c respectively. (Note different graph scale).

With VGs at 40%c, MaPFlow again overestimates the performance whilst OpenFoam underpredicts lift. Q^{3}UIC and VGFlow fair reasonably well in predicting the lift polar, but $C_{L,max}$ is over- and underestimated, respectively. Interestingly, Q^{3}UIC also appears to capture the stepwise lift drop after $C_{L,max}$. Comparing the pressure distributions for $\alpha = 16°$ for the

measured and predicted separated zones explains the different maximum lift characteristics for this airfoil. This again highlights the difficulties in the prediction of separated flow and its consequence for practical purposes.

4. Discussion and concluding remarks

Measurements from two wind energy type airfoils equipped with passive vortex generators have been used to benchmark the performance of computational codes in light of growing interest in these flow control devices. Predictions for transitional flow on the DU97W300 compare quite well without control devices. However, roughened surfaces pose modelling problems, observed on both airfoils. Unless models account for the physical presence of roughness, this issue will likely persist when assessing "fully-turbulent" airfoil flows and requires further attention.

Some effects of the VGs on airfoil performance are captured well, limited by classical issues with the prediction separated flows [32]. The experimental loads were indirectly obtained through model and wake pressure measurements. The immediate post-stall region presents issues with data interpretation due the the 3D flow nature and both experimental and computational (2D, low AR 3D) results should be interpreted with caution. Balance measurements would offer a better indication of the average flow over the wing in this regime. The same can be said of the periodic VG flow; the provision of reliable and representative polar data with these devices is not as trivial as the simplicity of the devices would suggest.

The tools show some discrepancies in the prediction of the magnitude and position of $C_{L,max}$, and hence, the extent of the linear range, which is a vital property for design and optimisation. The prediction of $C_{L,max}$ is even more complicated with VGs because it represents a critical balance between the decaying vortex system and the incipient separation. As suggested in Spalart et al. [33], investigations into the cause of this will likely require consideration of dedicated turbulence modelling, considering the complex turbulent structure of the vortices.

Wind turbines operate in a unique regime of very high Re at low Mach. The DU97W300 airfoil used for this study is typical of root/midboard sections, featuring a relatively high thickness for structural suitability. The thinner NTUA T18 might be encountered further outboard. A $10MW$ turbine can present a Reynolds regime of $10 - 20 \cdot 10^6$ and Ma up to 0.3. The general effect of Reynolds number would be to improve the maximum lift and minimum drag characteristics of the airfoils as boundary layers become thinner. Computationally, this would impose stricter meshing requirements. Local flow velocities at the tips of large rotors can exceed 100 $\mathrm{m\,s^{-1}}$ but there are normally other restrictions capping these tips speeds, such as noise limitations. The incompressibility assumption in current practice would likely still hold at Ma = 0.3, avoiding unwanted shock phenomena and associated compressibility drag [34]. The influence of Re on the coherent vortical flow induced by the VGs is less obvious, but careful management of vortex instabilities and breakdown is probably of most interest. For instance, Velte et al. [35] recently observed an atypical vortex transition at low Re number without changes in the flow topology. At higher Reynolds numbers, coupled with strong pressure gradients posed by thicker blades, further unstable vortex regimes may arise [36, 37]. These phenomena could lead to premature vortex breakdown and a loss of flow control ability. The stability of wall-bounded vortex systems has not been studied exhaustively and further investigations appear necessary. Notwithstanding, the experimental conditions used in the present comparisons are considered relevant and issues highlighted in this paper also pertain to full scale flows.

In conclusion, the added complexity and computational cost of fully resolved CFD for VG flows appears to offer only marginal improvements over well calibrated, simplified codes such as Q^3UIC and VGFlow. However, at present, experimental data for estimating robust tuning parameters covering a wide range of airfoils, device configurations and flow conditions are limited. Therefore, as an intermediary approach, the BAY-model is a promising solution which can potentially capture the effects of VGs on airfoils.

Acknowledgements
The work has been performed within the AVATAR project, initiated by the European Energy Research Alliance (EERA) and carried out under the FP7 program of the European Union.

References
[1] State of Green, `https://stateofgreen.com/en/news/the-world-s-biggest-wind-turbines-opened-in-denmark` (accessed: 25-05-2016)
[2] AVATAR Project Site, `http://www.eera-avatar.eu/` (accessed: 10-02-2016)
[3] van Rooij R P J O M and Timmer W A 2003 *Journal of Solar Energy Engineering* **125** 468–478
[4] Lin J C 2002 *Review of research on low-profile vortex generators to control boundary-layer separation* vol 38
[5] Ashill, P R and Fulker, J L and Hackett K C 2005 *Aeronautical Journal* **109** 205–232 ISSN 00105317
[6] Liu J, Piomelli U and Spalart P R 1996 *Journal of Fluid Mechanics* **326** 151 ISSN 0022-1120
[7] Spalart P R, Shur M L, Strelets M K and Travin A K 2015 *Flow, Turbulence and Combustion* ISSN 1386-6184
[8] Bender, EE, Anderson, BH, Yagle P 1999 *3rd Joint ASME/JSME Fluids Engineering Conference, San Francisco, CA.* March
[9] Jirasek A 2005 *Journal of Aircraft* **42**(6) 1486–1491
[10] Stillfried F V, Wallin S and Johansson A V 2012 *AIAA Journal* **50**(4) 855–866 ISSN 0001-1452
[11] Velte C M, Hansen M O L and Okulov V L 2008 *Journal of Fluid Mechanics* **619** 167 ISSN 0022-1120
[12] Kerho M and Kramer B 2003 *41st Aerospace Sciences Meeting and Exhibit, Aerospace Sciences Meetings, AIAA 2003-211* January
[13] Skrzypiński W, Gaunaa M and Bak C 2014 *Journal of Physics: Conference Series* **524** 012034 ISSN 1742-6596
[14] Manolesos M and Prospathopoulos J 2015 CFD & experimental database of flow devices. AVATAR Task 3.1, February
[15] Ferreira C, Salcedo A G, Baldacchino D and Aparicio M 2015 Development of aerodynamic codes for modelling of flow devices on aerofoils and rotors AVATAR Task 3.2
[16] Timmer W and van Rooij R P J O M 2003 *Journal of Solar Energy Engineering* **125**(4) 488–496
[17] Manolesos M and Voutsinas S G 2015 *Journal of Wind Engineering and Industrial Aerodynamics* **142** 130–148 ISSN 01676105
[18] Manolesos M and Voutsinas S G *Wind Energy* **17**(9) ISSN 1099-1824
[19] Manolesos M, Papadakis G and Voutsinas S G *Journal of Physics: Conference Series* **524** 012029
[20] Ramos-García N, Sørensen J N and Shen W Z 2014 *Wind Energy* **17**(12) 1957–1984
[21] Michelsen J 1992 Basis3D-platform for development of multiblock PDE solvers. Tech. Rep. AFM 92-05 TU Denmark
[22] Michelsen J 1994 Block structured multigrid solution of 2D & 3D elliptic PDE's. Tech. Rep. AFM 94-06 TU Denmark
[23] Sørensen N N 1995 *General purpose flow solver applied to flow over hills,* Ph.D. thesis Risø-R-827-(EN), Denmark.
[24] Leonard B P 1979 *Computer methods in applied mechanics and engineering* **19**(1) 59–98
[25] Menter F R 1993 *AIAA 23rd Fluid Dynamics, Plasmadynamics, and Lasers Conference, 93-2906*
[26] Michelsen J A Forskning i aeroelasticitet EFP-2001, chapter beregning af laminar-turbulent omslag i 2d og 3d, page 73 Tech. rep.
[27] Mack L M 1977 Transition and laminar instability Tech. rep. Jet Propulsion Laboratory
[28] Papadakis G and Voutsinas S 2014 *Journal of Physics: Conference Series*
[29] Nikolaou I G, Politis E S and Chaviaropoulos P K 2005 *Journal of Solar Energy Engineering* (2) 223 ISSN 01996231
[30] Jasak H 1996 *Error Analysis and Estimation for the Finite Volume Method with Applications to Fluid Flows* Ph.D. thesis Imperial College, University of London
[31] Florentie L, Van Zuijlen A and Bijl H 2014 *11th World Congress on Computational Mechanics, WCCM 2014, 5th European Conference on Computational Mechanics, ECCM 2014 and 6th European Conference on Computational Fluid Dynamics, ECFD 2014* pp 7187–7198
[32] Spalart P R and Venkatakrishnan V 2016 *The Aeronautical Journal* **120** 209–232 ISSN 2059-6464
[33] Spalart P R, Shur M L, Strelets M K and Travin A K *Flow, Turbulence and Combustion* ISSN 1386-6184
[34] Madsen H A, Bergami L and Rasmussen F (Eds) 2013 *INNWIND Task 2.1.1, New aerodynamic blade designs* New aerodynamics rotor concepts specifically for very large offshore wind turbines Tech. Rep. September
[35] Velte C M, Okulov V L and Hansen M O L 2011 *Physics of Fluids* **23** 1–4 ISSN 10706631
[36] Novak F and Sarpkaya T 2000 *AIAA Journal* **38**(5) 825–834 ISSN 0001-1452
[37] Escudier M 1988 *Progress in Aerospace Sciences* **25**(2) 189–229 ISSN 03760421